Heating Mechanism of Building Components Exposed to a Localized Fire -FDM Thermal Analysis of a Steel Beam under Ceiling-

T WAKAMATSU
Institute of Construction Technology
Kumagai Gumi Corporation
1043 Onigakubo, Tsukuba, Ibaraki 305, Japan

Y HASEMI
Department of Architecture and Architectural Engineering School of Science and Engineering
Waseda University
3-4-1 Ookubo, Shinjuku, Tokyo 169, Japan

ABSTRACT

Previously, we have conducted measurements of heat flux and temperature distribution of the H-shape beam installed beneath a ceiling and exposed to a localized fire source. From the results of the experiment, heat flux distribution on every part of the beam was formulated. In this paper ,the temperature distributions were computed by the finite different method using experimental heat flux data and compared with results of the experiments to evaluate the applicability of the analytical technique. The result shows that when compared with the experimental data, the temperature distribution on the axial direction of the member can be predicted with about 15% error in the range of 0.5m from the stagnation point, and with 20% error or less in other positions. In order that this model may be applied to an actual building, we assume two cases; one is that the temperature is calculated with the experimental data of heat flux approximated by a functional equation, and the other is a case that the experimental data is input in the model directly as mentioned above; and these two cases are compared with each other in their accuracy. In the same scheme, several kinds of metal material properties data were used in the calculation to know the heating conditions which may achieve the allowable range of temperature required in the current regulation .

NOMENCLATURE

A: sectional area of beam (m^2)
A_b: surface area of the section dx (m^2)
A_{bd}: area of the under surface of the lower flange of the section dx (m^2)
A_{bu}: area of the upper surface of the lower flange of the section dx(m^2)
Au: area of upper flange of the section dx(m^2)
As: area on which the upper flange contacts with the ceiling of the section dx(m^2)
Aw: area of web of the section dx(m^2)
CP_c: specific heat of ceiling material(kJ/kgK)
CP: specific heat of beam material(kJ/kgK)
Cp_0: specific heat of ambient air(kJ/kgK)
D: dimensions of heat source (m)
dx: distance of elements (m)
g: gravity acceleration (m/s^2)
H: vertical distance between heat source surface and ceiling surface (m)
H_B: height from the heat source surface to beam's lower flange (m)
H_C: height from heat source surface to ceiling (m)
H_S: height from the lower edge of the beam to the floor (m)
L_B: length of the flame which flows along the under surface of the lower flange (m)
L_C: length of the flame which flows along the under surface of the ceiling (m)
h: the convection part of heat transfer coefficient from the beam surface to the ambient air (kW/m^2K)

$h$ceil : the convection part of heat transfer coefficient from ceiling upper surface to ambient air(kW/m^{2}K)
L_f: the height of unconfined flametips (m)
T_a: temperature of the ambient air (K)
T_g: temperature of the measurement surface of the heat flux gage (K)
T_s: surface temperature of the specimen (K)
Q: heat release rate of heat source (kW)
Q*: dimensionless heat release rate assuming a characteristic length-scale D
Q_{HB}*:dimensionless heat release rate assuming a characteristic length-scale H_B
q: net heat flux to specimen surface (kW/m^2)
$q(i)$: heat flux (experimental value) to the element $d(i)$.
q_{bd} (i):heat flux to the under surface of the lower flange (experimental value kW/m^2)
q_{bu} (i):heat flux to the upper surface of the lower flange (experimental value kW/m^2)
q_g: heat flux measured by heat flux gage (kW/m^2)
q_u (i) heat flux to the under surface of the upper flange (experimental value kW/m^2)
q_w (i) heat flux to the web (experimental value kW/m^2)
z': empirical virtual source depth(m)
δ c: thickness of ceiling material(m)
ε_1: emissivity of specimen surface
ε_2: emissivity of heat flux gage
ε_c : emissivity of the ceiling upper surface
θ a : temperature of ambient air(K)
$\theta(i)$:temperature of a element $d(i)$
λ : thermal conductivity of beam member (kW/mk)
λ c : thermal conductivity of ceiling (kW/mk)
ρ : density of beam member (kg/m^3)
ρ_0 :density of ambient air (kg/m^3)
ρ c :density of ceiling material
σ : Stefan-Boltzmann constant

INTRODUCTION

If for a building, we intended to carry out a fire safety design rationally, the design should be performed by considering its specific fire-heating properties various buildings ; given by a fully developed fire, but also the systematic arrangement of structural members which are exposed to a localized heating. Yokobayashi and Hasemi measured heating conditions of a flat ceiling and a steel beam under the ceiling and exposed to a localized fire source .[1),2)] From the results of the experiment , heat flux distribution on every part of the beam was formulated as a function of flame length and distance from the fire source to the member , within error of $\pm$20%. By the previous paper[3)], with regard to a beam under the ceiling which was exposed to the localized heating, we made a FEM-based numerical calculation of temperature responses using the heat flux data which was obtained by experiment, and this numerical model was verified for its validity by comparing the numerical results of temperature with those obtained through the experiment. In this report, we could positively demonstrate the practical feasibility of our FEM-based model to predict temperature responses of members, and we also proposed a correction method of heat flux data, and showed a heat transfer coefficient under the experimental conditions. However, when implementing a FEM analysis by using a personal computer, we experienced that the memory capacity is not sufficient even for a relatively simple model ; much time was needed for the construction of a calculation model and for calculation. If we assume a beam which is heated only locally in fire , it is known from the comparison of heat flux to every parts of the beam on the same vertical section that there is no significant temperature distribution due to the thermal conductivity of metals. even in the event that there is an especially intensified heat flux distribution on upper and lower flanges and on the web ; paying an attention to this fact, we consider that it is possible to treat this phenomenon macroscopically with finite different methods. From this viewpoint, for the same specimen, we here propose a more simplified numerical model which is based upon FDM to predict temperatures of the member, and discuss its validity by comparison with the results of the experiments.

FDM MODEL
Analysis model

As a heat transmission conception, an H-shaped steel member, (hereinafter refereed to as beam) is located under the ceiling, which, as shown in Fig. 1, and the center of the beam is heated by a fire source on the floor. Considering a car parking structure we see frequently in parking areas, the beam directly bears a floor not a ceiling, but, the floor and ceiling, when considered in their material properties, have almost no difference in the effect on the temperature properties of the beam, so we placed a board of ceiling material on the beam. The ceiling used is a rectangular parlite board 1.8×3.6 (m), 24mm thick, and the beam thereunder, placed in the longitudinal direction of the ceiling, is a 3.6m long, 150×75×5×6 (mm) H-shaped ordinary bare steel beam as shown in Fig.1. In the case of our FEM analysis, considering its symmetrical form of the specimen, we prepared a 1/4 three dimensional, transient thermal analysis model representing the ceiling and beam. A temperature analysis model based upon FDM is shown in Fig.2(a). A rectangular prism model for analysis was constructed neglecting the sectional shape of the beam, which has the same surface area and the same volume as those of the H-shaped beam. At this calculation model, we considered heat transfer in a linear temperature field along in the beam's axial direction ; a transient temperature calculation was carried out for the half of the whole. Taking into account the fact that the thermal conductivity of the ceiling is lower than the beam (steel) , we used a simplified model ; our FDM model only considers the portion of the ceiling contacting the beam's upper flange. This calculation model is divided into 13 elements in the axial direction only, at the same intervals in right and left from the heat flux measurement point shown in Fig.2(b). The point just above the heat source (hereinafter refereed to as stagnation point) and the ends of the beam, because there is an insulation boundary on the measurement point, are treated as the width of the half of the other portion as shown in the figure. For the portions 90cm or more from the stagnation point, virtual measurement points are provided considering that the measurement interval is 2 times larger than that for the other portions. So the interval of elements should be same as that of the elements of other portions which is 7.5(cm) at the both edges and 15(cm)at other portions.

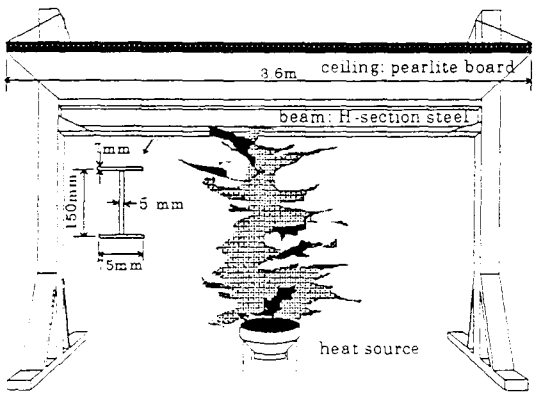

Fig. 1 Summary of the experiment

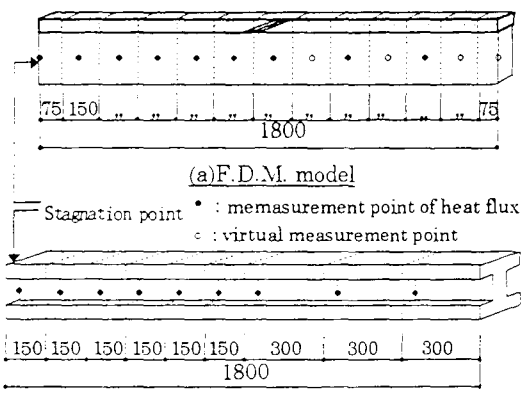

Fig. 2 Dimensions of the beam and measurement position

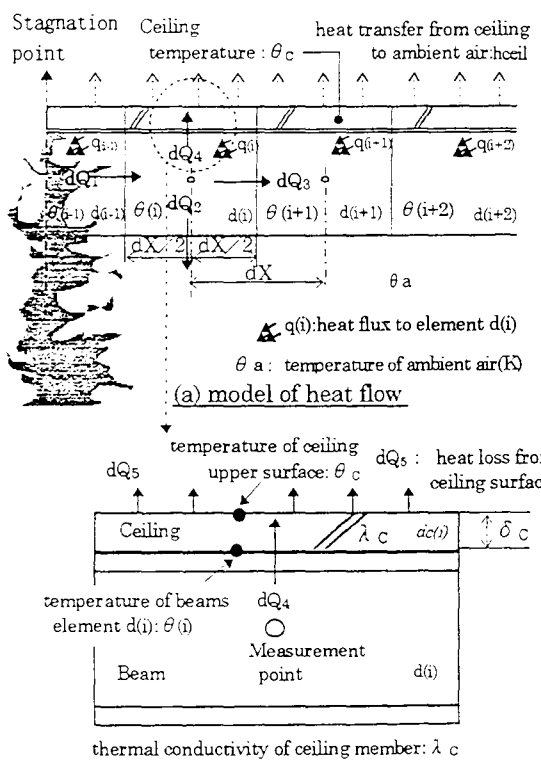

Fig. 3 Heat balance

Heat balance

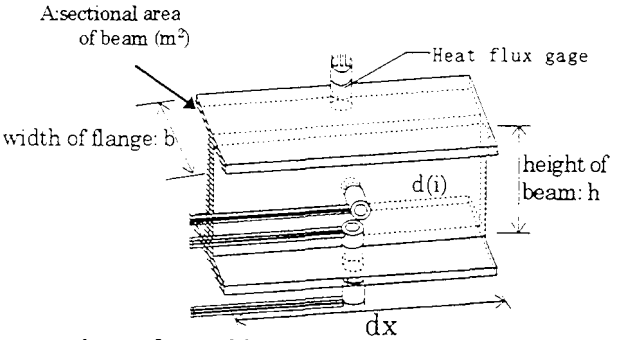

area of upper flange of the section dx : Au=dx×b
area of the upper surface of the lower flange of dx : Abu=dx×b
area of the under surface of the lower flange of dx : Abd=dx×b
area of web of the section dx : Aw=2×dx×h

Fig. 4 Measurement position of heat flux

The heat balance in the calculation model was modeled as shown in Fig. 3(a) and (b). In this model, FDM was carried out at steps of *dt* second in infinitesimal time. In the FDM, during the second *dt* of infinitesimal time, the temperature of each element for the beam and ceiling is treated as constant. Furthermore, the edges of the specimen and the ceiling are considered as insulation boundary. If in this temperature-calculating model, the heat flux entering each element is expressed as positive, that outgoing from the element as negative ; the heat amount having a positive value is a heat flux q*(i)* which reaches at the beam from outside and the heat amount dQ_1 which is transferred in conduction from the neighboring elements of higher temperatures. Details of the experiments are discussed in Literature[2] ; in the experiment, the measurement of heat flux was carried out at the interval above, on the upper and lower surface of the lower flange, on the surface of the web and the lower surface of the upper flange as shown in Fig. 4. In the FDM, each of the elements including the virtual measurement points is given an average of the values at its neighboring measurements in left and right sides. For other elements, no interpolation is applied to the data ; the heat flux data at various measurement points are respectively multiplied by the area of the portion concerned, and their total values is used as input data. Now, if we pay attention to a certain element *d(i)*, the input data of heat flux q*(i)* to the element can be expressed

$$q_{(i)}=q_{bd(i)}\times A_{bd}+q_{bu(i)}\times A_{bu}-q_{w(i)}\times A_{w}-q_{u(i)}\times A_{u} \quad \text{.....(1)}$$

In Fig. 3(a), assuming that the temperature of *d(i)* is $\theta(i)$ and that of the element d*(i-1)*is $\theta(i-1)$, the heat dQ_1 which, during *dt* second, flows into *d(i)* by thermal conduction from *d(i-1)* neighboring the element *d(i)*, is given by the following equation :

$$dQ_1=(\lambda/dx)\cdot(\theta(i-1)-\theta(i))\cdot A\cdot dt \quad \text{.....(2)}$$

In the same way, the heat which, during *dt* second, flows out by thermal conduction from *d(i)* to the neighboring *d(i+1)*, may be represented by

$$dQ_3=(\lambda/dx)\cdot(\theta(i)-\theta(i+1))\cdot A\cdot dt \quad \text{.....(3)}$$

When assuming that the heat which, during *dt* second, moves in heat transmission from the element *d(i)* to the ambient air, is dQ_2, the convection heat loss dQ_{2c} can be express by

$$dQ_{2c}=h\cdot A_b\cdot(\theta(i)-\theta a)\cdot dt \quad \text{.....(4)}$$

The heat loss due to radiation dQ_{2R} can be given by

$$dQ_{2R}=\varepsilon\cdot\sigma\cdot A_b\cdot(\theta(i)^4-\theta a^4)\cdot dt \quad \text{.....(5)}$$

Therefore, dQ_2 is obtained by the following equation,

$$dQ_2=dQ_{2c}+dQ_{2R} \quad \text{.....(6)}$$

where

ε : emissivity (in this case ,0.9)

With the temperature of the ceiling member $\theta c(i)$, the heat dQ_4 which, during the time *dt*, is conducted to the element *dc(i)* of the ceiling from the element d*(i)* by thermal conduction is expressed by

$$dQ_4=(\lambda c/\delta s)\cdot As\cdot(\theta(i)-\theta c(i))\cdot dt \quad \text{.....(7)}$$

The heat loss dQ_5 from the upper surface of the ceiling to the ambient air over the time span of dt second can be determined by

$$dQ_5 = h\text{ceil} \cdot As \cdot (\theta c(i) - \theta a) \cdot dt - \varepsilon c \cdot \sigma \cdot As \cdot (\theta c(i)^4 - \theta a^4) \cdot dt \quad \text{.....(8)}$$

where

ε_c : emissivity of the ceiling upper surface (in this case, 1.0).

Our FEM method [3] theoretically calculated the value of the convection part of heat transfer coefficient from the ceiling upper surface to the ambient air, using an experimental equation [4] which, in the case of a rectangle with its open circumference, represents the turbulence heat transfer coefficient of the upward flow of air from the rectangle. In this calculation proposed here, we use the value 0.0072(kW/m^2K)for the convection part of heat transfer coefficient.

Using the equations (7) and (8), the ceiling temperature $\theta c(i)(dt)$ in a time span dt (second) from the initial state (ceiling temperature: $\theta c(i)$) may obtained by equation (9), with the ceiling material specific heat CPc and ceiling material density ρ_C.

$$\theta c(i)(\mathrm{dt}) = \theta c(i) + (dQ_4 - dQ_5) / (CP_C \cdot \rho_C \cdot As \cdot \delta c) \cdot \mathrm{dt} \quad \text{.....(9)}$$

From this, the heat balance at a element $d(i)$ can be expressed by

$$q(i) \cdot \mathrm{dt} + dQ_1 - dQ_2 - dQ_3 - dQ_4 = CP \cdot \rho \cdot A \cdot dx \cdot (\theta c(i)(\mathrm{dt}) - \theta(i)) \quad \text{.....(10)}$$

Therefore, the temperature $\theta(i)(dt)$ of the element $d(i)$ after an infinitesimal time dt elapsing from the initial state can be given by

$$\theta(i)(\mathrm{dt}) = \theta(i)(0) - (q(i) \cdot \mathrm{dt} - dQ_1 - dQ_2 - dQ_3 - dQ_4) / (CP \cdot \rho \cdot A \cdot dx) \quad \text{.....(11)}$$

With the calculation model we propose here, we calculated $\theta(i)(dt)$ in the equation (11), letting the initial temperature $\theta(i)(0)$ be 18 degrees, and adding successively each temperature increase at each time step dt.

Material properties

With regard to the thermal conductivity and specific heat of a beam member (of ordinary steel) for analyzing temperatures, we considered the temperature-dependency of thermal conductivity and specific heat from equations (12) and (13), letting steel material temperature be T(K). Concerning the thermal conductivity and specific heat of the ceiling material, as it is known that temperature dependency does exert almost no influence on analysis results, we use $\lambda c = 3.588 \times 10^{-5}$(kW/mK), Cpc = 0.144(kJ/kgK). Furthermore, the density of steel material and inorganic-fibrous board are respectively constant, that is 7850 kg/m^3 and 789 kg/m^3.

$$\lambda = 0.06 - 6.25 \times 10^{-8} \times (T-273.16)^2 \quad \text{.....(12)}$$

$$CP = 0.4815 + 7.997 \times 10^{-7} \times (T-273.16)^2 \quad \text{.....(13)}$$

Correction of heat flux data

The net heat transfer to the specimen surface depends upon the surface temperature of the specimen itself. However, the heat flux gages used were of water cooling type, so there was a considerable temperature difference between the specimen surface temperature (Ts) and that (Tg) of the measurement surface of heat flux gage.

If the data of the measurement surface of the heat flux gage is used as it is, some error may occur due to the temperature difference mentioned above. Modeling of a heat balance on the specimen surface as shown Fig.5 makes it possible to express the net heat flux to the specimen surface (q) by the following equation ;

$$q = q_{EXP} - h(Ts - Ta) - \varepsilon_1 \sigma (Ts^4 - Ta^4) \quad \text{.....(14)}$$

Here, assuming that the difference in heat transfer coefficient h due to the temperature difference between heat flux gage and specimen surface can be neglected, the heat flux (q_g) by heat flux gage is given by

$$q_g = q_{EXP} - h(Tg - Ta) - \varepsilon_2 \sigma (Tg^4 - Ta^4) \quad \text{.....(15)}$$

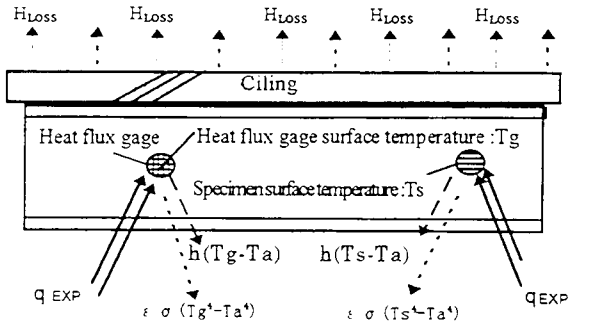

Fig.5 Modeling of a heat balance

From Eq.(14) and (15),we can estimate the net heat flux (q) to the specimen surface, using the heat flux (qg) by heat flux gage, according to

$$q = q_g - h(T_S - Tg) - \varepsilon_1 \sigma (Ts^4 - Ta^4) + \varepsilon_2 \sigma (Tg^4 - Ta^4) \quad \text{.....(16)}$$

Considering the case the flat ceiling is heated locally (Yokobayashi et al.,1996)[1], we implemented comparisons between temperature analysis and experiment according to the finite element method using the experiment value of qg; after repeating tries and errors, we could find a heat transfer coefficient of h = 0.01(kW/m^{2}K) which may ensure a good conformity between calculation and experiment. Even with the conditions slightly different for the beam, we used this value for Eq.(4) and (16) . The value of 30(°C), which is measured for the cooling water which passes through the heat flux gage, is inputted as the temperature (Tg) of the surface measured by heat flux gage, and for the temperature (Ta) of the ambient air, 16(°C) was inputted.

CALCULATION RESULTS

Comparison of calculation results with experimental results

To the calculation model shown above, the heat flux measured at each spot is substituted to calculate the temperature distribution in the axial direction of the beam ; the values obtained by this procedure were compared with the experimental values to verify the validity of the model. The calculation results and measured values are shown in Figure 6 to Figure 11. The X axis represents the distance r(m) from the stagnation point and the line with rectangular points shows the measured values of the lower and upper flanges; the broken line represents the calculation results and the solid line shows a calculation result which is obtained by the functional equation which will be discussed later. The experimental and calculation values are those obtained 7 minutes or 20 minutes after the start of experiment, under the conditions in which all the spots of the members reaches an almost steady state in temperature.

From the graphs, we can know that the most of the calculation values shown by the broken line are included in the range of temperature measurements of the upper and lower flanges, except for the cases the heat release rates of 130 (kW) and 160 (kW). By comparing the calculation value with the measurement value for the stagnation point, we can know the following; under the conditions that the heat release rate is 150,200 (kW) and the distance from the heat source to the member is 1.0(m), the calculation value is approximately 10% lower than the measurement value at the lower flange , but they coincide well with each other under the other conditions. In the range of 0.25 to 0.5m from the stagnation point , with the heat release rate 130, 160 (kW) and with the heat source-member distance 0.6 (m) , the calculation value is about 25% higher than the measurement value at the lower flange.

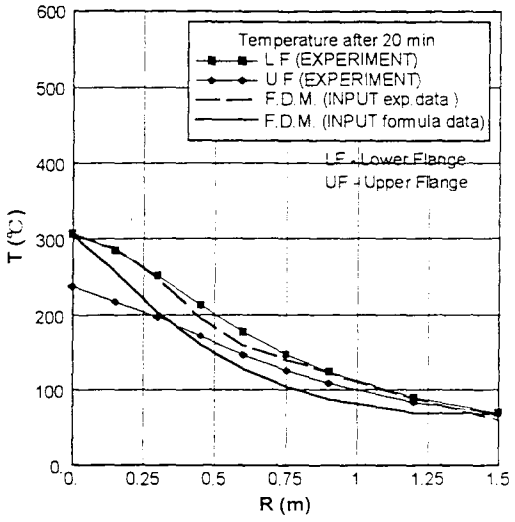

Fig.6 Comparison between calculation and experimental values (Q=100kW, H_B=1.0m)

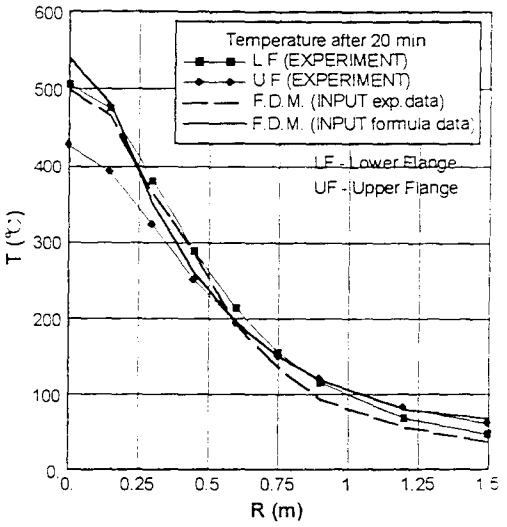

Fig.9 Comparison between calculation and experimental values (Q=95kW, H_B=0.6m)

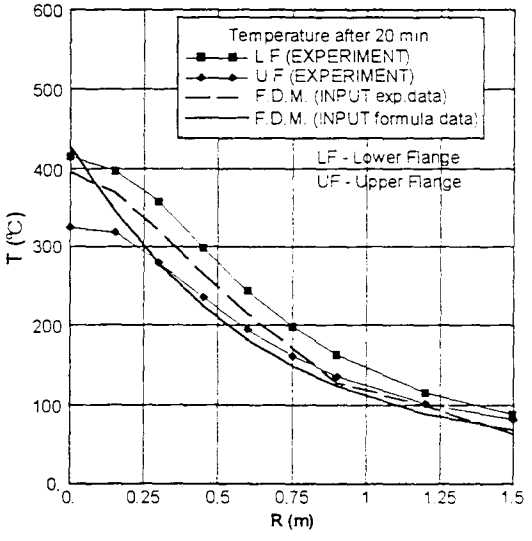

Fig. 7 Comparison between calculation and experimental values (Q=150kW, H_B=1.0m)

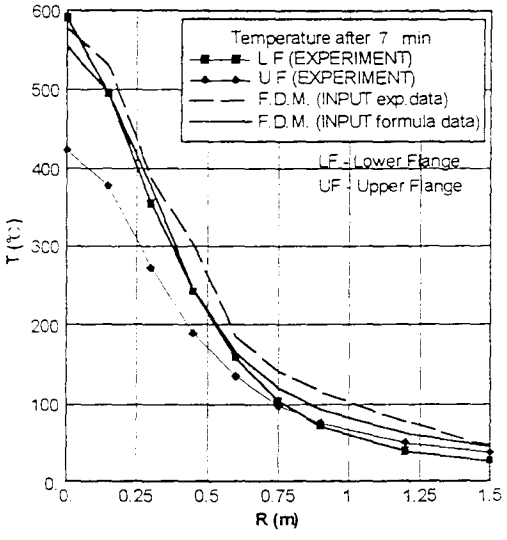

Fig. 10 Comparison between calculation and experimental values (Q=130kW, H_B=0.6m)

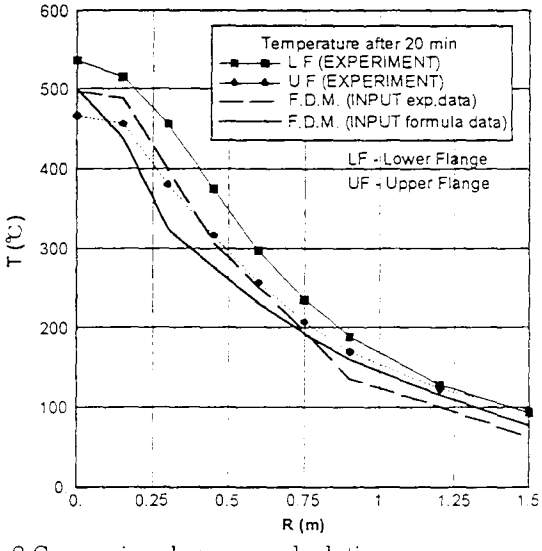

Fig. 8 Comparison between calculation and experimental values (Q=200kW, H_B=1.0m)

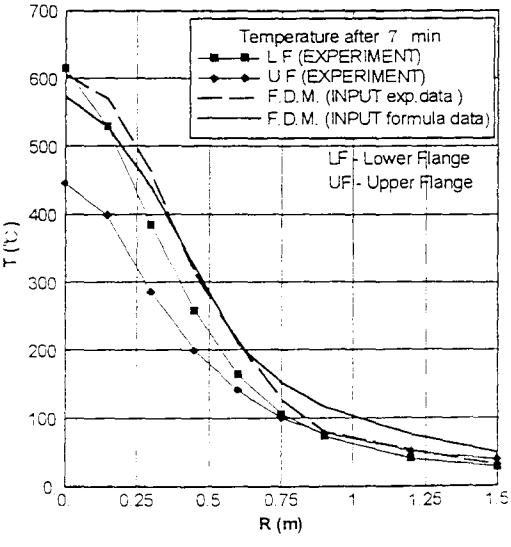

Fig.11 Comparison between calculation and experimental values (Q=160kW, H_B=0.6m)

Calculation by recurrence formula

When for a actual building in which an localized fire may occur, we predict temperature distribution on a beam member by this method, it is necessary to estimate the heat flux to the beam. Yokobayashi and Hasemi have shown that the heat flux distribution on every part of the beam exposed to a localized fire can be represented as a function of the radial distance from the stagnation point (r) which is normalized by the flame length (L_B or L_C),virtual source depth (z') and the height (H_B or H_C).[2)]

In the relation above, H_B denotes the distance from the burner surface to the bottom of the beam, H_C the distance from the burner surface to the under surface of the ceiling, and L_B the length of a flame from the stagnation point, which flows along the lower surface of the beam , and L_C the length of a flame from the stagnation point, which flows along the under surface of the ceiling .(z') is a correction value given by the following equations, using the conception of an empirical virtual source depth.

$$z' = 2.4D(Q^{*2/5} - Q^{*2/3}) \quad (Q^* < 1) \qquad .....(17)$$

$$z' = 2.4D(1 - Q^{*2/5}) \quad (Q^* \geqq 1) \qquad .....(18)$$

where Q^* is the dimensionless heat release rate given by

$$Q^* = Q/\rho_0 C_{P0} \theta a g^{1/2} D^{5/2} \qquad ..... (19)$$

They also have shown that the flame length (L_B)and (L_C) are well represented as a function of the dimensionless heat release rate (Q_{HB}*) calculated by the equation (19).

$$Q_{HB}^* = Q/\rho_0 C_{P0} \theta a g^{1/2} H_B^{5/2} \qquad ..... (20)$$

The experimental data of Yokobayashi and Hasemi is approximated, and the heat flux at each spot which is given by a functional equation is substituted into this calculation model to determine temperatures; the temperatures obtained by this method are compared with the results obtained by substituting directly the experimental heat flux data into the calculation model to know the magnitude of difference between the two methods above. Fig.-12 shows, as an example of experimental data , the relation between heat flux to the downward surface of the lower flange and the radial distance from the stagnation point which is normalized by the flame length(L_B) and virtual source depth (z') . In the experiment, we measured heat flux at the four points: upper and lower surfaces of the lower flange, surface of web and downward surface of the upper flange. The data scatter more significantly in the range of $(r+H_B+z')/(L_B+H_B+z') > 1$(where no flame exist) than in the range of $(r+H_B+z')/(L_B+H_B+z') < 1$ (where flame exist). Therefore, with $(r+H_B+z')/(L_B+H_B+z') = 1$ as a discrimination condition, the heat flux for calculation is separately introduced for the range of $(r+H_B+z')/(L_B+H_B+z') < 1$ and that of $(r+H_B+z')/(L_B+H_B+z') > 1$. These two range are regressed into an approximate expression. In addition, we can know that the heat flux to the lower surface of the lower flange is larger than that at other positions, and as shown in Fig.-12, the gradient of heat flux is larger in the experimental condition of H_B=0.6(m) than H_B=1.0(m). In order to examine the relationship between the heat release rate and the flame length, we looked into a relationship between (L_B) and

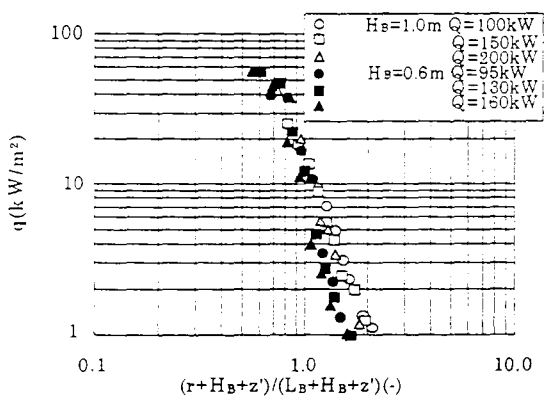

Fig. 12 Measured heat flux to the under surface of the lower flange

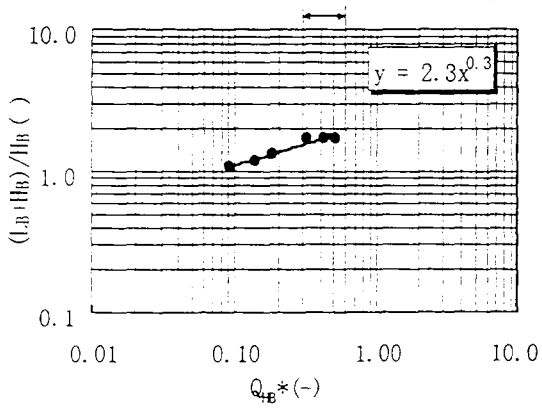

Fig. 13 Relation between Q_{HB}* and $(L_B+H_B)/H_B$(-)

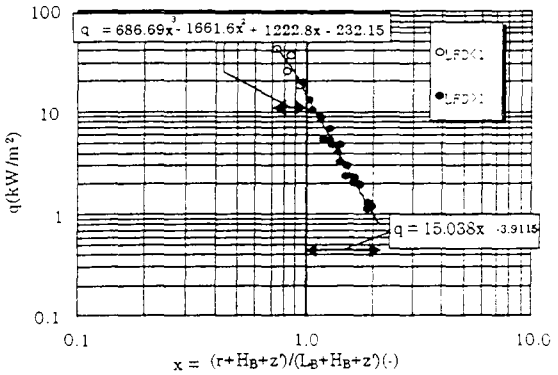

Fig. 14 Approximation of the heat flux to the under surface of the lower flange (HB=1m)

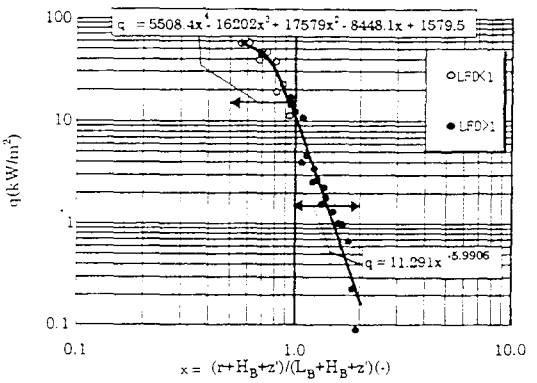

Fig. 15 Approximation of the heat flux to the under surface of the lower flange (HB=0.6m)

the dimensionless heat release rate (Q_{HB}*) the experimental data [2] of Yokobayashi and Hasemi ; it is observed that $(L_B+H_B)/H_B$(-) increases lineally with(Q_{HB}*) < 0.3 or less, but $(L_B+H_B)/H_B$(-) approached the plateau in the domain of (Q_{HB}*)>0.3. The experimental conditions are that H_B(m) is 1.0(m)when (Q_{HB}*)is less than 0.3 and 0.6(m)when (Q_{HB}*)is from 0.3 to 0.5. These phenomena denote that when Q_{HB}* is 0.3 or more the length L_B of the flame flowing along the under surface of the lower flange increases slowly, and the amount of the heat flux to the lower surface of lower flange does not rise anymore. Considering the above conditions, it is anticipated that if the data of the heat flux to the under surface of the lower flange is approximated in the same way as that for the other portions, the error will significant; under these circumstances, we decided to use the group of experimental data with H=0.6 (m), when Q_{HB}*> 0.3, and the group of experimental data with H=1.0 (m), when Q_{HB}*$\leqq$0.3, on the basis of Q_{HB}*. Furthermore, we applied the discrimination condition above, that is $(r+H_B+z')/(L_B+H_B+z')=1$, to these groups of data to regress them, using two approximating equations. These four approximation curves and approximating equations of heat flux data to the lower surface of lower flanges are given in Figs. 14 and 15. In the same way, Figs 16, 17 and 18 show the approximation curves and equations to represent the estimation of heat flux to the upper surface of the lower flange, the surface of web and the lower surface of the upper flange. In the figures, the white points denote the experimental data of the range of $(r+H_B+z')$ (L_B+H_B+z') < 1 and the black points the other ranges. With regard to the approximation curve, we selected and used the one which is the nearest to the 1, by comparing the square values of moment generation function.

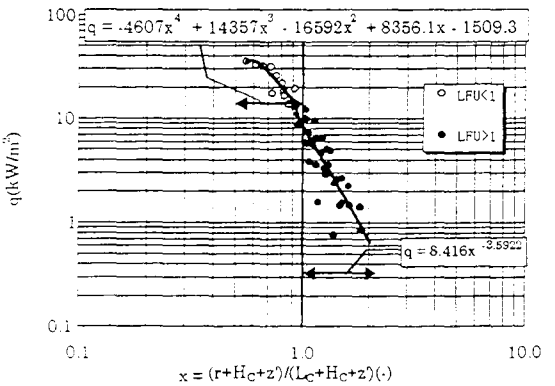

Fig. 16 Approximation of the heat flux to the upper surface of the lower flange

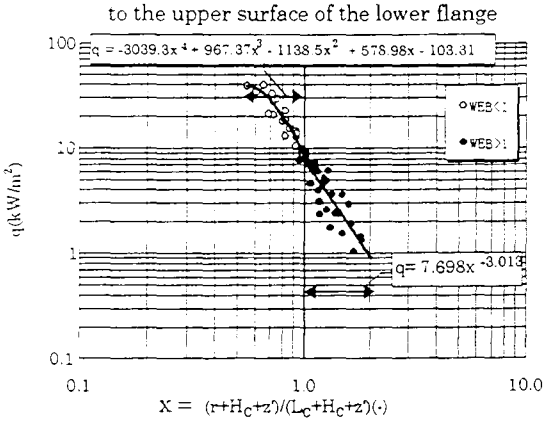

Fig. 17 Approximation of the heat flux to the web surface

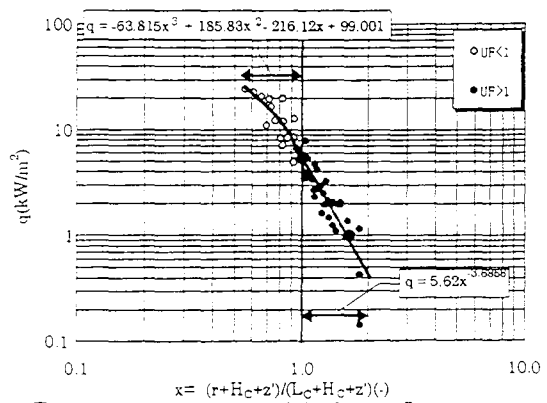

Fig. 18 Approximation of the heat flux to the under surface of the upper flange

CALCULATION RESULTS BY REGRESSION EQUATION

By the regression equation above, we calculated the heat flux to the measurement position of each element, and the value thus obtained, was used to the calculation model. The results of calculation are shown by solid line in Figs 6 to 11. The comparison of the figures indicates that at the stagnation point, the difference between the calculation value and the experimental value of the lower flange is approximately $\pm 10\%$. At the locations 0.3 (m) or more apart from the stagnation point, the three experiments with H_B = 1.0 (m) demonstrated that at the upper flange, the calculation value is lower than the experimental value; in the case of 200 (kW), the maximum of the errors is about 20% at the position of 0.3 (m) from the stagnation point. The calculation values with H_B=0.6(m) agree well with the experimental values of the lower flange, except for the case of the experimental conditions with the heat release rate of 160 (kW). With regard to H_B =1.0(m) in experimental condition, the conformity with the experimental values of the lower flange is relatively bad, when compared with the results from the calculation model to which the experimental heat fluxes are directly introduced, but as for H_B=0.6 (m), the conformity is confirmed to be relatively good.

COMPARISON WITH THE METALS OF OTHER KINDS

With this calculation model, the prediction of temperatures was carried out with metals of deferent kinds such as aluminum, fire-resistant steel, etc. Their temperature behavior was compared under the conditions up to the limit temperature. The current regulation requires that the allowable temperature of the ordinary steel should be 450(℃), in maximum, and 350(℃) in average; the allowable temperature of the fire-resistant steel is specified 600(℃) or less. As concerns the stress deformation characteristics of a structure when exposed to a fire, the specified fire resistance performance can be maintained at 600(℃) or less for the structure of ordinary steel, at about 350(℃) or less for the structure of aluminum alloy, and at the temperatures less than about 800(℃) for the stainless steel[5]. Fig.-19, assuming the same calculation conditions presented above, shows a relation between Q and H_B (m) which is obtained by the calculation model, where Q is defined as being required to maintain the member's temperature lower than the limit, and H_B is the distance limit to satisfy the temperature requirement mentioned above . In this calculation . We assumed that the sectional dimensions of the members are H-150×75×5×7(mm) and 3.6(m) long ,and these beams are heated at its center by a heat source of 0.5(m) in diameter. With regard to the heating conditions, the heat release rate and the distance from the heat source to the beam are changed considering $1 \leqq Lf/H \leqq 2.5$; this condition was confirmed by Yokobayashi and Hasemi's experiment with a ceiling [1]; they reported that the ratio of Lf (m) and H(m) can be expressed in a relation of $1 \leqq Lf/H \leqq 2.5$, when the member is kept exposed to a localized fire. As concerns material properties, 40-FR is used as a fire-resistant steel, and for the aluminum, we used the density data [4] of pure metal; for thermal conductivity and specific heat, their temperature-dependency was considered. Each point in the figure indicates the temperature condition in which the temperature at the moment the calculation value reaches a steady state may be maintained less than the limit temperatures shown in Fig.19. From the figure, we can know that the graph is inclined more sharply inversely with the limit temperature, and when the metals are different in kinds, even under the same temperature limit, the values Q and H_B are different to each other. We conducted the same survey on the stainless steel of pure metal, and it is found that the material never exceeds the limit temperature of 800(℃) in the heating conditions of $1 \leqq Lf/H \leqq 2.5$.

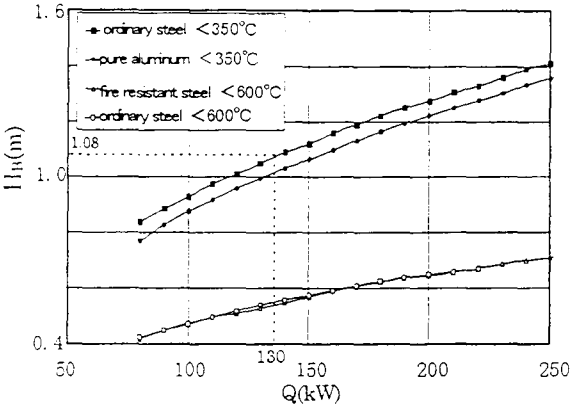

Fig. 19 Heating conditions of the metals of other kinds under the limit temperature

APPLICATIONS

Now, with Fig. 19, we consider a case we are requested to calculate the necessary height of H_B of an open car parks. The model for this calculation may be deemed as representing , in cross-section , 1/3 of the typical steel beam normally used in this kind of structures. Since the heat release rate of the 1/3 model is about 130 (kW) when the maximum heat release rate of a car is 2000 (kW) ; and the temperature of the ordinary steel beam is required to be restricted to under 350(℃). To satisfy this requirements, we can know from the figure that it is necessary that the distance from the bottom of the beam to the heat source should be 1.08 m or more.

Therefore, the actual distance from the lower edge of the beam to the floor

H_S (m) is expressed as $H_S>1.08\times3+0.5=3.74$ (m), assuming that the heat source of the car is 0.5 m from the floor.

CONCLUSIONS

We examined the validity of FDM based numerical model which is to analyze the temperature distributions along the beam installed beneath a ceiling and exposed to a localized fire. From the results of the calculation, following conclusions can be drawn.

(1) By inputting the values of the experimental data of heat flux to their corresponding elements for the model, we could confirm that our model is able to calculate the actual temperature with 10% error for the stagnation point, and with about 25% error or less for the other positions.

(2) The experimental data of heat flux are regressed in ten approximation equations by using the discrimination equation, according to the position of the beam member and the heating conditions; the difference between the calculation value by these recurrence formula and the experimental one is approximately 10% or less at the stagnation point. At the positions 0.3 m or more from the stagnation point, the difference is considerable with the heat generation rate of 200 (kW) and 160 (kW), and the maximum error is 25% at the position 0.3 m from the stagnation point, with 160 (kW).

Based upon the discussions above, we can say that our calculation model can predict the temperature response with almost same accuracy as that of the finite element method.

(3) If the data are available concerning the material properties of aluminum members and fire-resistant steel , etc., our calculation model is able to easily formulate a relation between the heat release rate and the floor height, which is required to keep the member's temperature lower than the limit value.

For this calculation, we used the member of a dimensional ratio which is frequently available on the market; but if for the members of other dimensional ratios, the relation between the their heat generation rate and the heat source-member distance can be graphed as in Fig.19, we expect that it will be possible to simply examine the required fire-protection and the required floor height.

ACKNOWLEDGMENTS

This research program is implemented as a joint study by Building Research Institute, Ministry of Construction, and by Institute of Construction Technology, Kumagagi-gumi.

REFERENCES

1) Yokobayashi,Y.,Hasemi,Y.,Wakamatsu,T.and Wakamatsu ,T., 1996 "Heating Mechanism of Flat Ceiling Exposed to Localized Fire, - An Introduction to The Fire Safety Design of Building Structures Exposed to Localized Fire " ,Journal of Structural and Construction Engineering, Transactions of AJI , No .484 (in Japanese)

2)Wakamatsu, T., Hasemi, Y., Yokobayashi,Y., A.V. Ptchelintsev ,1996"Experimental Study on the Heating Mechanism of a Steel Beam exposed to a Localized Fire "; proceedings, Interflam '96 Cambridge

3)Wakamatsu, T., Hasemi, Y.,A.V.Ptchelintsev,1997"Heating Mechanism of Building Components Exposed to a Localized Fire-FEM Thermal and Structural Analysis of a Steel Beam Under Ceiling - " ,Proceedings, OMAE '97 Yokohama , or

Wakamatsu, T., A.V. Pchelintsev, Hasemi, Y. 1997 "Numerical Prediction of Thermal Response of Building Components Exposed to Localized Fires,-FEM Thermal Analysis of a Steel Beam -" Journal of Structural and Construction Engineering, Transactions of AJI , No .497 ,July (in Japanese)

4)Thermal Transmission Documents (4th revision); Mechanical Institute of Japan, Maruzen Co., Ltd. 1986)

5)Building Research Institute, Ministry of Construction, Japan Light Metal Association, Japan Exterior Industries : Comprehensive Technological Development Project, Development of new materials and new technologies for construction projects, Guidelines on the fire protection design of aluminum alloy structures., March 1994(in Japanese)